

Dynamical nucleus-nucleus potential at short distances

Yongying Jiang,¹ Ning Wang ^{*},¹ Zhuxia Li,² and Werner Scheid³

¹*Department of Physics, Guangxi Normal University, Guilin 541004, P. R. China*

²*China Institute of Atomic Energy, Beijing 102413, P. R. China*

³*Institute for Theoretical Physics at Justus-Liebig-University, D-35392 Giessen, Germany*

Abstract

The dynamical nucleus-nucleus potentials for fusion reactions $^{40}\text{Ca}+^{40}\text{Ca}$, $^{48}\text{Ca}+^{208}\text{Pb}$ and $^{126}\text{Sn}+^{130}\text{Te}$ are studied with the improved quantum molecular dynamics (ImQMD) model together with the extended Thomas-Fermi approximation for the kinetic energies of nuclei. The obtained fusion barrier for $^{40}\text{Ca}+^{40}\text{Ca}$ is in good agreement with the extracted fusion barrier from the measured fusion excitation function, and the depth of the fusion pockets are close to the results of time-dependent Hartree-Fock calculations. The energy dependence of fusion barrier is also investigated. For heavy fusion system, the fusion pocket becomes shallow and almost disappears for symmetric systems and the obtained potential at short distances is higher than the adiabatic potential.

* Corresponding author

E-mail address: wangning@gxnu.edu.cn

I. INTRODUCTION

The synthesis of super-heavy elements (SHEs) has been studied for many years both theoretically and experimentally [1–4]. Up to now the super-heavy nuclei are uniquely synthesized through fusion reaction including "cold" fusion reaction with lead and bismuth targets [3] and "hot" fusion with actinide targets [4]. The study of the dynamical process in fusion reactions especially the nucleus-nucleus potential is of great importance for the synthesis of SHEs. Experimentally, the fusion barrier distributions can be directly obtained from the measured fusion excitation functions, with which the information of the nucleus-nucleus potential around the fusion barrier can be obtained. Fig.1(a) shows the nucleus-nucleus potential calculated with different models for $^{40}\text{Ca}+^{40}\text{Ca}$. We can see that the obtained barrier heights with different models are close to each other and all of them are comparable with the extracted mean barrier height, while the calculated nucleus-nucleus potentials at short distances are quite different with different models. It is known that the adiabatic and diabatic approximations lead to different nucleus-nucleus potentials especially at short distances and thus to different fusion paths and different mechanisms of fusion reactions. Both approximations are frequently applied to the study of the synthesis of super-heavy nuclei [1, 10]. For understanding the fusion mechanism of a heavy system, it is important and necessary to study the nucleus-nucleus potential at short distances, with which one could get information on the fusion path and the formation probability of the di-nuclear system in reactions leading to super-heavy nuclei.

For description of heavy-ion fusion reactions, some theoretical models have been developed. The fusion coupled channel model is a powerful tool to calculate the fusion excitation function and to investigate the influence of nuclear structure effects on the fusion cross sections [11–13]. On the other hand, the microscopic dynamics model such as time dependent Hartree Fock (TDHF) model [14, 15] and the improved quantum molecular dynamics (ImQMD) model [16, 17] are widely applied to study the dynamical behavior of fusion process. The ImQMD model is a semi-classical microscopic dynamics model and is successfully used for intermediate-energy heavy-ion collisions and for heavy-ion collisions at energies near the Coulomb barrier [16–19]. In the ImQMD model the dynamical effects such as the dynamical deformation, neck formation, etc, are microscopically and self-consistently taken into account. Recently, the model has been applied to the study of the dynamical barrier

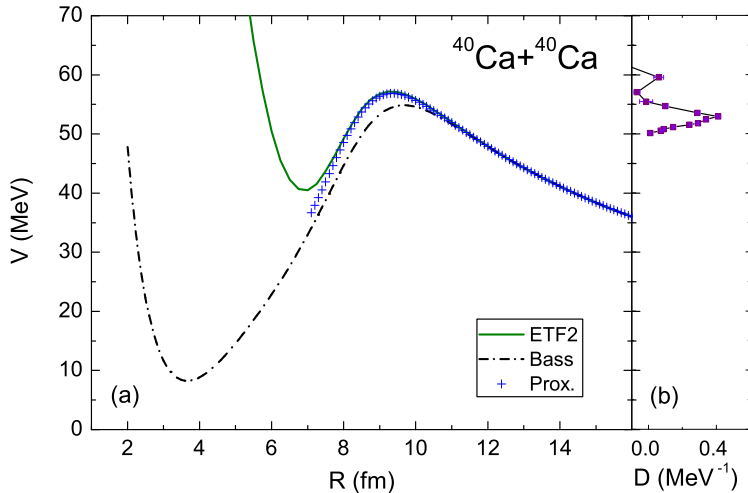


FIG. 1: (Color online) (a) The nucleus-nucleus potential as a function of the center-to-center distance R between two nuclei for the reaction $^{40}\text{Ca}+^{40}\text{Ca}$. The solid curve denotes the results of Skyrme energy density functional together with the extended Thomas-Fermi (ETF2) approximation [5]. The dash-dotted curve and the crosses denote the Bass potential [6] and the proximity potential [7], respectively. (b) The fusion barrier distribution extracted from the measured fusion excitation function [8] (see Eq.(9) of Ref.[9]).

of a heavy system [20], of mass parameters [21], and of the strongly damped process of $^{238}\text{U}+^{238}\text{U}$ [22, 23]. In this paper we carefully investigate the kinetic energies of nuclei based on the extended Thomas-Fermi approximation with which the dynamical fusion barrier is accurately obtained. The paper is organized as follows: In Sec. II, the ImQMD model will be briefly introduced. In Sec. III, some calculated results on the kinetic energies of nuclei and the nucleus-nucleus potential for $^{40}\text{Ca}+^{40}\text{Ca}$, $^{48}\text{Ca}+^{208}\text{Pb}$ and $^{126}\text{Sn}+^{130}\text{Te}$ will be presented. Finally, a summary is given in Sec. IV.

II. THE IMPROVED QUANTUM DYNAMICS MODEL

In the ImQMD model, the same as in the original QMD model [24], each nucleon is represented by a coherent state of a Gaussian wave packet. Through a Wigner transformation, one can get the one-body phase space distribution function for N -distinguishable particles

(see [16, 24] for details). The density distribution function ρ of a system reads

$$\rho(\mathbf{r}) = \sum_i \frac{1}{(2\pi\sigma_r^2)^{3/2}} \exp\left[-\frac{(\mathbf{r} - \mathbf{r}_i)^2}{2\sigma_r^2}\right]. \quad (1)$$

Where, σ_r represents the spatial spread of the wave packet. The propagation of nucleons is governed by Hamiltonian equations of motion under the self-consistently generated mean field:

$$\dot{\mathbf{r}}_i = \frac{\partial H}{\partial \mathbf{p}_i}, \dot{\mathbf{p}}_i = -\frac{\partial H}{\partial \mathbf{r}_i}. \quad (2)$$

Where, \mathbf{r}_i and \mathbf{p}_i are the centers of i-th wave packet in the coordinate and momentum space, respectively. The Hamiltonian H consists of the kinetic energy and the effective interaction potential energy:

$$H = T + U, \quad (3)$$

$$T = \sum_i \frac{\mathbf{p}_i^2}{2m}. \quad (4)$$

The effective interaction potential energy includes the nuclear interaction potential energy and the Coulomb interaction potential energy,

$$U = U_{loc} + U_{Coul}, \quad (5)$$

with

$$U_{loc} = \int V_{loc}(\mathbf{r}) d\mathbf{r}. \quad (6)$$

Where $V_{loc}(\mathbf{r})$ is the potential energy density which is obtained by the effective Skyrme interaction and taken as the same as that in Ref.[17]

$$V_{loc} = \frac{\alpha}{2} \frac{\rho^2}{\rho_0} + \frac{\beta}{\gamma + 1} \frac{\rho^{\gamma+1}}{\rho_0^\gamma} + \frac{g_{sur}}{2\rho_0} (\nabla\rho)^2 + g_\tau \frac{\rho^{\eta+1}}{\rho_0^\eta} + \frac{C_s}{2\rho_0} (\rho^2 - \kappa_s (\nabla\rho)^2) \delta^2, \quad (7)$$

where $\delta = \frac{\rho_n - \rho_p}{\rho_n + \rho_p}$ is the isospin asymmetry. Inserting expression (1) together with (7) into (6), we obtain the interaction potential energy

$$\begin{aligned} U_{loc} = & \frac{\alpha}{2} \sum_i \frac{\rho_i}{\rho_0} + \frac{\beta}{\gamma + 1} \sum_i \left(\frac{\rho_i}{\rho_0}\right)^\gamma + \frac{g_0}{2} \sum_i \sum_{j \neq i} f_s \frac{\rho_{ij}}{\rho_0} \\ & + g_\tau \sum_i \left(\frac{\rho_i}{\rho_0}\right)^\eta + \frac{C_s}{2} \sum_i \sum_{j \neq i} t_i t_j \frac{\rho_{ij}}{\rho_0} (1 - \kappa_s f_s), \end{aligned} \quad (8)$$

where

$$\rho_i = \sum_{j \neq i} \rho_{ij} = \sum_{j \neq i} \frac{1}{(4\pi\sigma_r^2)^{3/2}} \exp\left[-\frac{(\mathbf{r}_i - \mathbf{r}_j)^2}{4\sigma_r^2}\right], \quad (9)$$

TABLE I: Parameters set IQ2.

Parameter	$\alpha(\text{MeV})$	$\beta(\text{MeV})$	γ	$g_0(\text{MeVfm}^2)$	$g_\tau(\text{MeV})$	η	$C_s(\text{MeV})$	$\kappa_s(\text{fm}^2)$	$\rho_0(\text{fm}^{-3})$
IQ2	-356	303	7/6	7.0	12.5	2/3	32.0	0.08	0.165

$$f_s = \frac{3}{2\sigma_r^2} - \left(\frac{\mathbf{r}_i - \mathbf{r}_j}{2\sigma_r^2} \right)^2, \quad (10)$$

and $t_i = 1$ for protons and -1 for neutrons respectively. The parameters set IQ2 [18] (see Table 1) is adopted in this work. The Coulomb energy is written as the sum of the direct and the exchange contribution, and the latter being taken into account in the Slater approximation [25, 26]

$$U_{Coul} = \frac{e^2}{2} \int \frac{\rho_p(\mathbf{r})\rho_p(\mathbf{r}')}{|\mathbf{r} - \mathbf{r}'|} d\mathbf{r}d\mathbf{r}' - e^2 \frac{3}{4} \left(\frac{3}{\pi} \right)^{1/3} \int \rho_p^{4/3} d\mathbf{r}. \quad (11)$$

To describe the fermionic nature of the N-body system and to improve the stability of an individual nucleus, the phase space occupation constraint method [27] and the system-size-dependent wave-packet width $\sigma_r = 0.09A^{1/3} + 0.88$ fm [18] are adopted. The phase space occupation constraint is an effective approach to improve the momentum distribution of nuclear system [16, 27]. In this approach, the phase space occupation number of each particle is checked at each time step. If the phase space occupation number is larger than 1 for particle i , i.e. $\bar{f}_i > 1$, the momentum of the particle i are randomly changed by a series of two-body elastic scattering between i and its partner which guarantee that the total momentum and total kinetic energy are conserved in the procedures. In the ImQMD model, the new sample for the momenta of the particles is constrained by the Pauli-blocking probability [27] as in the usual two-body collision process. Actually, the momenta of two particles obtained in this way not only influence the motion of particles of the system in this step but also the further more steps. It is unknown whether the system will be in the most suitable motion path. In this work, we perform one more step further, i.e. we calculate the total energy of the system at step t and also the total energy $E(t + \Delta t)$ at the next time step ($t + \Delta t$) simultaneously. If the value of $E(t + \Delta t)$ obviously deviates from that of $E(t)$, the two-body elastic scattering procedure is re-executed. The number of times of the re-executing process is small (about $0 \sim 4$) at each time step for fusion reactions. This additional constraint can further improve the stability of an individual nucleus (reducing

the spurious emission of nucleons), and is helpful for the study of the formation process of the compound nuclei which lasts several thousand fm/c or longer. We have checked that the total energy of system is well conserved for thousands of fm/c with this new procedure.

III. RESULTS

In this section we first study the kinetic energies of a series of nuclei. Then, we calculate the nucleus-nucleus potential in fusion reactions based on the extended Thomas-Fermi approximation.

A. Kinetic energies of nuclei

We first study the kinetic energy of a series of nuclei in the ground state from ^{16}O to ^{259}No . Based on the extended Thomas-Fermi (ETF) approximation [28], the kinetic energy of a free Fermi gas can be expressed as

$$E_k = \frac{\hbar^2}{2m} \int \tau(\mathbf{r}) d\mathbf{r} = c_k \langle \rho \rangle^{2/3} + \frac{\hbar^2}{2m} \frac{1}{36} \int \frac{(\nabla \rho)^2}{\rho} d\mathbf{r} + \dots \quad (12)$$

with the kinetic energy density $\tau(\mathbf{r})$ and the coefficient $c_k = \frac{\hbar^2}{2m} \frac{3}{5} \left(\frac{3\pi^2}{2}\right)^{2/3}$. With the help of the ETF form of the kinetic energy for Fermi gas system in Eq.(12), we express the kinetic energy of an individual nucleus in the ImQMD model as

$$E_k^{\text{ETF}} \simeq c_0 \sum_i \rho_i^{2/3} + \frac{c_1}{\sum_i \rho_i} \sum_{i,j \neq i} f_s \rho_{ij} + c_2 N. \quad (13)$$

with $c_0 = 41.2 \text{ MeVfm}^2$, $c_1 = 4.8 \text{ MeVfm}^2$ and $c_2 = -1.0 \text{ MeV}$ for IQ2, which are determined by fitting the obtained kinetic energies of a series of nuclei with Eq.(4), see Fig.2. N is the particle number of the system under consideration. The expressions of ρ_i , ρ_{ij} and f_s are previously given in Eq.(9) and (10), respectively. The c_0 term of Eq.(13) represents the result of the Thomas-Fermi approximation (see the $\langle \rho \rangle^{2/3}$ term of Eq.(12)). The other terms give the corrections from the finite system effect.

We show the time average of the kinetic energy per particle for a series of nuclei in Fig. 2(a). Here we take 100 events for each nucleus. The solid and open circles denote the results with Eq.(4) and Eq.(13) which is based on the "ETF" approximation, respectively. Here, "ETF" means that the form of Eq.(13) is roughly obtained according to the extended Thomas-Fermi approximation. The crosses denote the results with the "TF" approximation

$$E_k^{\text{TF}} \simeq c_0 \sum_i \rho_i^{2/3}, \quad (14)$$

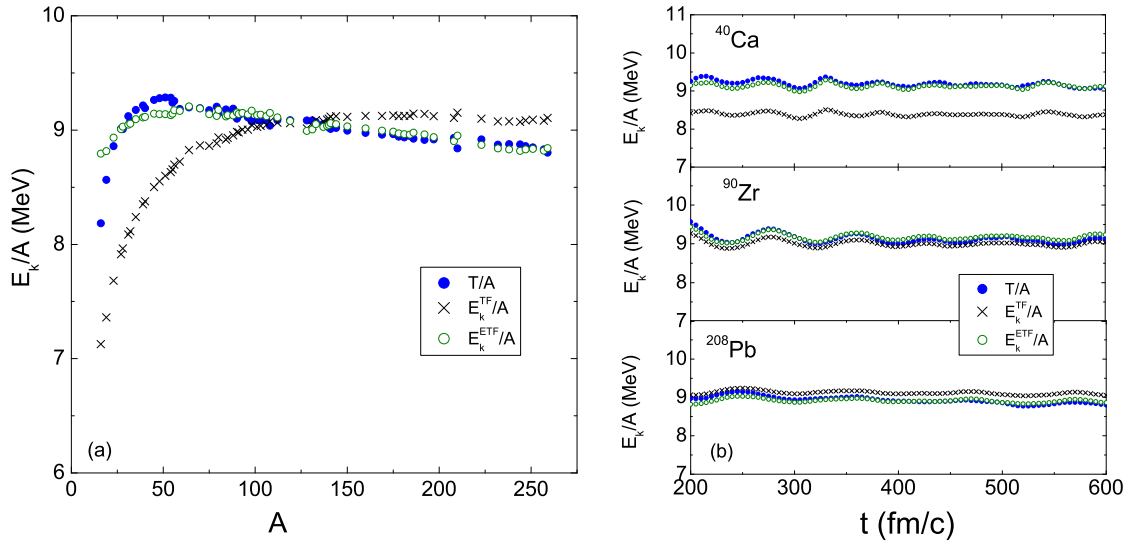


FIG. 2: (Color online) (a) Time average of the kinetic energy per particle for a series of nuclei. The solid circle, the open circle and the crosses denote the results with Eq.(4), (13) and (14), respectively. (b) The time evolution of the kinetic energy per particle for ^{40}Ca , ^{90}Zr , and ^{208}Pb .

in which the correction terms from the finite system effect are not taken into account. From the figure one can see that for the light nuclei ($A < 50$), the calculated kinetic energies with the "TF" approximation are much smaller than the values with Eq.(4), while for heavy nuclei ($A > 150$), the results with the "TF" approximation are slightly larger than those with Eq.(4). Only for the intermediate nuclei the results are in agreement with each other. The calculated kinetic energy with the "ETF" approximation is in good agreement with the values with Eq.(4) except for very light nuclei. From Fig.2, one can see that the "ETF" approximation can reasonably well describe the kinetic energy for finite nuclei. The time evolution of the kinetic energies per particle for nuclei ^{40}Ca , ^{90}Zr , and ^{208}Pb are shown in Fig. 2(b). The kinetic energies of these nuclei can be well described by the Eq.(13) based on the "ETF" approximation.

B. Nucleus-nucleus potential in fusion reactions

By using the ImQMD model, we can calculate the static and dynamical Coulomb barriers. In the calculation of the static Coulomb barrier which is based on the frozen density

approximation, the initial density distribution of the projectile and target is adopted. In the calculation of the dynamical Coulomb barrier, the realistic density distribution of the system which changes with time due to the interaction between nucleons is used. In this work, we concentrate on the calculation of the dynamical fusion barrier. We study the dynamical nucleus-nucleus potential V based on the "ETF" approximation for the kinetic energy. According to the energy conservation, we have

$$E_{c.m.} = T_R + V + E^* + T_{oth}, \quad (15)$$

where $E_{c.m.}$ is the incident center-of-mass energy, T_R is the relative motion kinetic energy of two colliding nuclei, which can be easily obtained in the ImQMD model since the position and momentum of each nucleon can be followed at every time step in this model, E^* is the excitation energy, T_{oth} is other collective kinetic energy, such as neck vibration. When the projectile and target nucleus are well separated ($R \gg R_1 + R_2$), the E^* and T_{oth} could be negligible which have been checked by the time-dependent Hartree-Fock (TDHF) calculations [14, 29], the nucleus-nucleus potential is thus expressed as

$$V_1 = E_{c.m.} - T_R. \quad (16)$$

Where, R_1 and R_2 are the charge radii of the projectile and the target nucleus, respectively, which are described by an empirical formula $R_i = 1.25A^{1/3}(1 - 0.2\frac{N-Z}{A})$ proposed in [30]. After the di-nuclear system is formed ($R < R_1 + R_2$), the nucleus-nucleus potential may be described by a way like the entrance channel potential [31]

$$V_2 = E_{tot}(R) - \bar{E}_1 - \bar{E}_2, \quad (17)$$

where $E_{tot}(R)$ is the energy of the composite system which is strongly dependent on the dynamical density distribution of the system obtained with the ImQMD model, \bar{E}_1 and \bar{E}_2 are the time average of the energies of the projectile and target nuclei, respectively. Here, the values of \bar{E}_1 and \bar{E}_2 are obtained from the energies of the projectile (like) and target (like) nuclei in the region $R_T < R < R_T + 8$. $R_T = R_1 + R_2$ is the touching point. R is the relative distance between the two nuclei, which is a function of time. In the calculation of $E_{tot}(R)$, \bar{E}_1 and \bar{E}_2 , Eq.(13) that is a function of local density is used for the description of the intrinsic kinetic energy of the system under consideration.

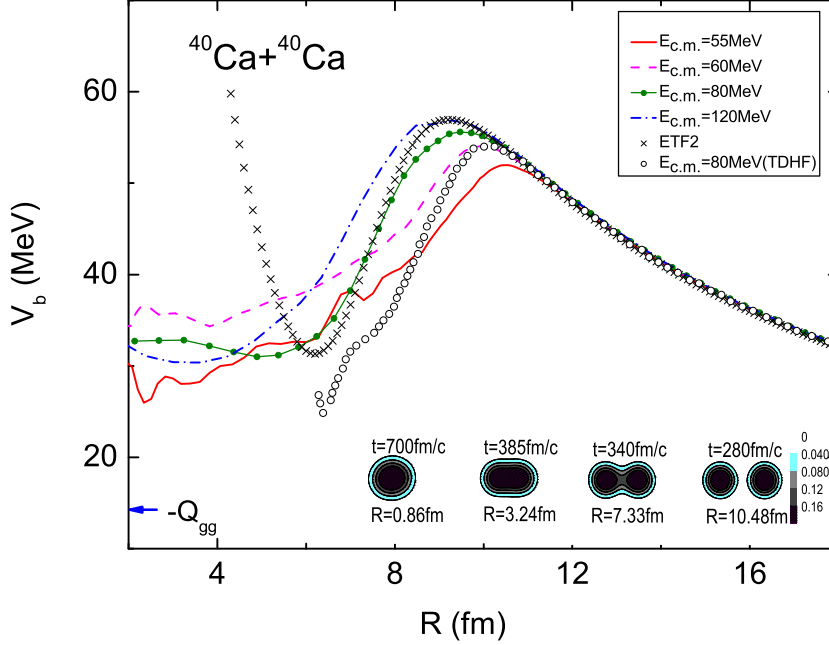


FIG. 3: (Color online) The dynamical nucleus-nucleus potential of $^{40}\text{Ca}+^{40}\text{Ca}$ at different incident energies $E_{c.m.}$. The crosses denote the entrance channel potential with the Skyrme energy density functional approach [5] which is based on frozen density approximation. The open circle denotes the results of TDHF [32] at $E_{c.m.}=80\text{MeV}$. The inserted sub-figures denote the the density distributions for this reaction at $E_{c.m.}=80\text{MeV}$ and different relative distances, respectively.

In this work, we write the nucleus-nucleus potential as a smooth function between V_1 and V_2 ,

$$V_b(R) = \frac{1}{2}\text{erfc}(s)V_2 + [1 - \frac{1}{2}\text{erfc}(s)]V_1 \quad (18)$$

where $\text{erfc}(s)$ is the complementary error function and

$$s = \frac{R - R_T + \delta}{\Delta R} \quad (19)$$

with $\delta=1\text{fm}$, $\Delta R=2\text{fm}$. The obtained nucleus-nucleus potential in Eq.(18) approaches to V_1 with the increase of the separation distance between two nuclei. On the contrary, $V_b(R)$ approaches to V_2 with the formation of the di-nuclear system and the decrease of the distance between two nuclei. To study the dynamical nucleus-nucleus potential, we create 500 reaction events for head-on collision of $^{40}\text{Ca}+^{40}\text{Ca}$ at several center-of-mass (c.m.) energies

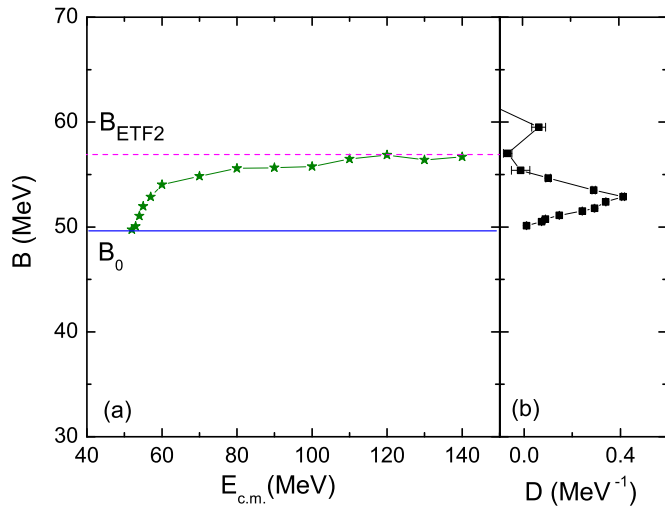


FIG. 4: (Color online) (a) Barrier height B for the reaction $^{40}\text{Ca}+^{40}\text{Ca}$ at different incident energies $E_{c.m.}$. The horizontal dashed and solid lines indicate the barrier height of the entrance channel potential based on the frozen density approximation [5] and the lowest barrier B_0 extracted from the fusion excitation function [8], respectively. (b) The same as Fig.1(b).

ranging from $E_{c.m.} = 52$ to 140 MeV. For each event, we evolve the reaction system for a time of 700 fm/c. The distance between the projectile and target at the initial time is set to 30 fm for this reaction. The scattering events at $t = 700$ fm/c are not involved in the calculation of the nucleus-nucleus potential. Fig. 3 shows the obtained dynamical nucleus-nucleus potential at different incident energies $E_{c.m.}$. The corresponding density distributions at $E_{c.m.}=80$ MeV and different relative distances are also shown in the sub-figures. Fig. 4 shows the average fusion barrier height B for the reaction $^{40}\text{Ca}+^{40}\text{Ca}$ at different $E_{c.m.}$. From the Fig. 3 and Fig. 4 we can see that the dynamical barriers depend on the incident energies. At energies around the Coulomb barrier, the dynamical barrier increases rapidly with the incident energy. With the further increase of the incident energy, the dynamical barrier approaches to the barrier height of the entrance channel potential (56.9 MeV) which is obtained with the Skyrme energy density functional together with the frozen density approximation [5]. This trend has also been found in [15, 20]. When the incident energy decreases gradually and down to $E_{c.m.} = 55$ MeV, the height of dynamical barrier falls to 52.0 MeV. With lower incident energy, the height of the dynamical barrier

approaches to about 50 MeV which is close to the height of the lowest barrier B_0 extracted from the fusion excitation function. In addition, it is encouraging that the obtained barrier height and the depth of the fusion pocket in this work are comparable with the results of the TDHF calculations [32]. The depth of the fusion pocket is about 25 MeV for this reaction system.

At very short distances between two nuclei, it is thought that the Q value of the fusion system may provide information of the nucleus-nucleus potential. One commonly defines the excitation energy for a reaction from the expression

$$-Q_{gg} = E_{c.m.} - E^*, \quad (20)$$

where Q_{gg} is the mass difference between the two initial nuclei and the combined system in its ground state. From Eq.(15) and Eq.(17), one can find that when the compound nucleus is well formed and the collective motion can be negligible one gets $V(R=0) = -Q_{gg}$, which is the result of the adiabatic nucleus-nucleus potential [10]. For the reaction $^{40}\text{Ca}+^{40}\text{Ca}$, we have $-Q_{gg}=14.3$ MeV. Actually, because the expression (20) is correct relative to the ground state of the composite system, it does not accurately describe the excitation energy relative to other intermediate transition states formed during the collision [32], the nucleus-nucleus potential obtained from the ImQMD model and the TDHF [32] at short distance does not exactly reach the value $-Q_{gg}$ since the composite system formed during the collision is far from a ground state.

With the same approach we studied the nucleus-nucleus potential for the reactions $^{48}\text{Ca}+^{208}\text{Pb}$ and $^{126}\text{Sn}+^{130}\text{Te}$ at energies above the Coulomb barrier. The corresponding values of $-Q_{gg}$ for these two reactions are 153.8 and 261.2 MeV, respectively. These two reactions lead to the same compound nucleus ^{256}No . Fig. 5 shows the calculated nucleus-nucleus potentials for these two reactions. The arrows denote the Bass barriers. From Fig. 5 we can see that the obtained barrier heights are close to the corresponding Bass barriers. The depth of the fusion pocket (about 7 MeV) for $^{48}\text{Ca}+^{208}\text{Pb}$ becomes much shallower than that of $^{40}\text{Ca}+^{40}\text{Ca}$ (about 25 MeV) and the fusion pocket for $^{126}\text{Sn}+^{130}\text{Te}$ almost disappears, which indicates that quasi-fission could easily occur in heavy fusion process especially for the more symmetric systems. Furthermore, we find that the nucleus-nucleus potentials for the reactions $^{48}\text{Ca}+^{208}\text{Pb}$ and $^{126}\text{Sn}+^{130}\text{Te}$ at short distances are much higher than the value of $-Q_{gg}$ and even higher than the Coulomb barrier, which is quite different from the case

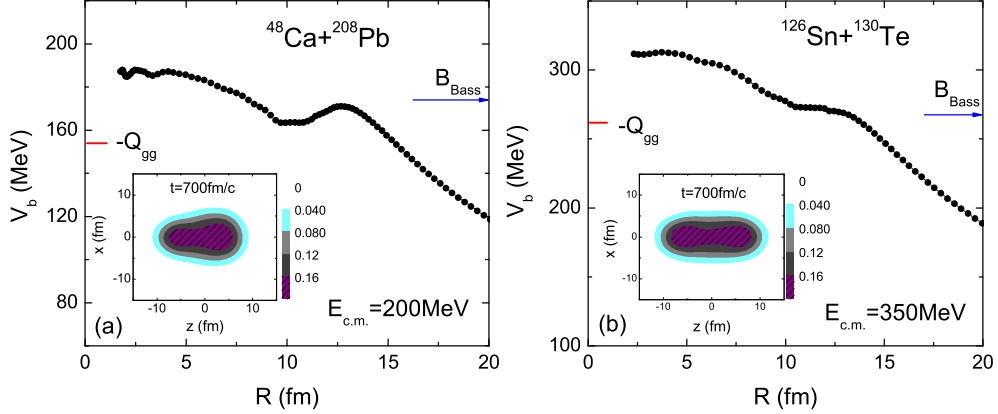


FIG. 5: (Color online) Dynamical nucleus-nucleus potentials for the reactions $^{48}\text{Ca}+^{208}\text{Pb}$ and $^{126}\text{Sn}+^{130}\text{Te}$ at an incident energy $E_{c.m.}=200\text{MeV}$ and $E_{c.m.}=350\text{MeV}$, respectively. The initial distance is set to 40 fm. The arrows denote the corresponding Bass barriers.

of $^{40}\text{Ca}+^{40}\text{Ca}$. These calculations indicate: 1) additional incident energy (so-called extra-push energy [2]) beyond the energy to overcome the Coulomb barrier may be required to form the compound nucleus for heavy fusion system and 2) the process of nucleon transfer between the projectile (like) and the target (like) could last for a period of time due to the appearance of the fusion pocket in di-nuclear system, which is the basic assumption of the di-nuclear system (DNS) model [1]. To see the fusion path, we also show the corresponding density distributions of the composite systems at $t = 700\text{fm}$ in the inserted sub-figures. One can see that the corresponding compound nuclei are not well formed at $t = 700\text{fm}$ for these two heavy fusion systems. The strongly deformed composite systems or called di-nuclear systems are formed at about $t = 350\text{fm}$ and can last hundreds even thousands fm/c for heavy fusion system, which is quite different from the case of light system such as $^{40}\text{Ca}+^{40}\text{Ca}$ in which the spherical composite system is well formed at $t = 700\text{fm}$ with the incident energies above the Coulomb barrier (see Fig.3). For $^{126}\text{Sn}+^{130}\text{Te}$, the composite system tends to undergo quasi-fission or fission. In Fig.6 we show the capture cross sections of these two reactions. The solid and open circles in Fig.6(a) denote the experimental data of $^{48}\text{Ca}+^{208}\text{Pb}$ in Ref.[33] and [34], respectively. The solid curves denote the results of an empirical barrier distribution approach which is based on the Skyrme energy-density

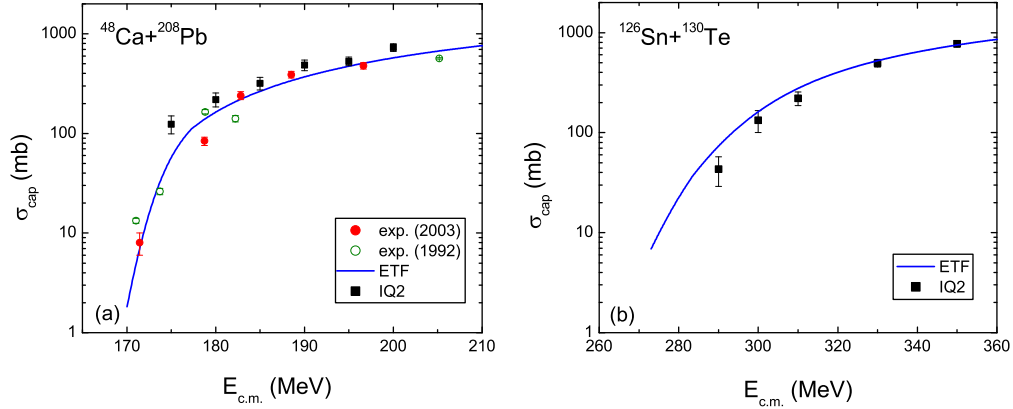


FIG. 6: (Color online) Capture cross sections for the reactions $^{48}\text{Ca}+^{208}\text{Pb}$ and $^{126}\text{Sn}+^{130}\text{Te}$. The open and solid circles in (a) denote the experimental data of $^{48}\text{Ca}+^{208}\text{Pb}$ [33, 34]. The solid curves denote the results of an empirical barrier distribution approach proposed in [5, 35]. The solid squares denote the results of the ImQMD model and the error bars denote the corresponding statistical error.

functional together with the extended Thomas-Fermi (ETF) approximation [5, 35]. The solid squares denote the results of the ImQMD model with IQ2 and the error bars denote the corresponding statistical errors. For the reaction $^{48}\text{Ca}+^{208}\text{Pb}$, the experimental data at energies above the Coulomb barrier can be reproduced acceptably well by the ImQMD model. Because the ImQMD model has difficulties to deal with the shell effects, the capture cross sections of $^{48}\text{Ca}+^{208}\text{Pb}$ at sub-barrier energies can not be described well. For $^{126}\text{Sn}+^{130}\text{Te}$, the calculated capture cross sections with the ImQMD model are comparable with the results of the empirical barrier distribution approach.

IV. SUMMARY

In summary, the kinetic energies of a series of nuclei have been studied with the ImQMD model together with the extended Thomas-Fermi (ETF) approximation which gives accurate results for finite nuclear system, especially for the light and heavy nuclei. Furthermore, with the "ETF" approximation for the kinetic energies we have studied the dynamical Coulomb barrier of the reaction $^{40}\text{Ca}+^{40}\text{Ca}$ at different incident energies. The results show that the dynamical Coulomb barrier strongly depends on the incident energy. With the increase of

the incident energy, the dynamical Coulomb barrier increases gradually and approaches to the entrance channel potential which is based on the frozen density approximation. The height of dynamical Coulomb barrier decreases with the decrease of the incident energy and approaches to the lowest barrier extracted from the fusion excitation function. The behavior of nucleus-nucleus potential at short distances for heavy system is obviously different from that of light systems. For heavy fusion systems, the depth of the fusion pocket becomes much shallower and the nucleus-nucleus potential at short distances are higher than the adiabatic potential. The capture cross sections for $^{48}\text{Ca}+^{208}\text{Pb}$ and $^{126}\text{Sn}+^{130}\text{Te}$ have also been studied with the ImQMD model. The calculated results are comparable with the results of the empirical barrier distribution approach. A systematic study of heavy fusion systems, such as the calculation of the potential energy surface of the composite system in the fusion process as a function of mass-asymmetry and the distance between two nuclei is in progress with the shell effects being taken into account.

ACKNOWLEDGEMENTS

This work is supported by the National Natural Science Foundation of China, Nos 10875031, 10847004 and 10979024, and the Innovation Project of Guangxi Graduate Education, No. 2009106020702M36.

-
- [1] G. G. Adamian, N. V. Antonenko, W. Scheid, et al., Nucl. Phys. A **633**, 409 (1998).
 - [2] C. Shen, G. Kosenko, and Y. Abe, Phys.Rev. C **66**, 061602(R) (2002).
 - [3] S. Hofmann and G. Münzenberg, Rev. Mod. Phys. **72**, 733 (2000).
 - [4] Yu. Ts. Oganessian, et al., Phys. Rev. C **70**, 064609 (2004).
 - [5] Min Liu, Ning Wang, et al., Nucl. Phys. A **768**, 80 (2006).
 - [6] R. Bass, Nuclear Reactions with Heavy Ions (Springer-Verlag, Berlin, 1980), p. 318.
 - [7] W. D. Myers and W. J. Świątecki, Phys. Rev. C **62**, 044610 (2000).
 - [8] H. A. Aljuwair, R. J. Ledoux, M. Beckerman, et al., Phys. Rev. C **30**, 1223 (1984).
 - [9] Ning Wang, Zhuxia Li and Werner Scheid, J. Phys. G: Nucl. Part. Phys. **34**, 1935 (2007).
 - [10] V. Zagrebaev, A. Karpov, et al., Phys. Part. Nucl., **38**, 469 (2007).
 - [11] K. Hagino, N. Rowley and A. T. Kruppa, Comp. Phys. Comm. **123**, 143 (1999).

- [12] Takatoshi Ichikawa, Kouichi Hagino, and Akira Iwamoto, *Phys. Rev. C* **75**, 057603 (2007)
- [13] Henning Esbensen and Şerban Mişicu, *Phys. Rev. C* **76**, 054609 (2007).
- [14] A. S. Umar and V. E. Oberacker, *Phys. Rev. C* **74**, 021601(R) (2006).
- [15] Kouhei Washiyama and Denis Lacroix, *Phys. Rev. C* **78**, 024610 (2008).
- [16] N. Wang, Z. Li and X. Wu, *Phys. Rev. C* **65**, 064608 (2002).
- [17] N. Wang, Z. Li, X. Wu, J.Tian, et al., *Phys. Rev. C* **69**, 034608 (2004).
- [18] N. Wang, Z. Li, X. Wu, et al., *Mod. Phys. Lett. A* **20**, 2619 (2005).
- [19] Y. Zhang, P. Danielewicz, M. Famiano, Z. Li, et al., *Phys. Lett. B* **664**, 145 (2008).
- [20] J. Tian, X. Li, X. Wu, Z. Li, and S. W. Yan, *Eur. Phys. J. A* **42**, 105 (2009).
- [21] K. Zhao, Z. Li, X. Wu, and Z. Zhao, *Phys. Rev. C* **79**, 024614 (2009).
- [22] J. Tian, X. Wu, K. Zhao, and Y. Zhang, Z. Li, *Phys. Rev. C* **77**, 064603 (2008).
- [23] Kai Zhao, Xizhen Wu, Zhuxia Li, *Phys. Rev. C* **80**, 054607 (2009).
- [24] J. Aichelin, *Phys. Rep.* **202**, 233 (1991).
- [25] J. C. Slater, *Phys. Rev.* **81**, 85 (1951).
- [26] J. Bartel and K. Bencheikh, *Eur. Phys. J. A* **14**, 179 (2002).
- [27] M. Papa, T. Maruyama, and A. Bonasera, *Phys. Rev. C* **64**, 024612 (2001).
- [28] M. Brack, C. Guet, and H. B. Hakanson, *Phys. Rep.* **123**, 275 (1985).
- [29] S. E. Koonin, et al., *Phys. Rev. C* **15**, 1359 (1977).
- [30] B. Nerlo-Pomorska and K. Pomorski, *Z. Phys. A* **348**, 169 (1994).
- [31] V. Yu. Denisov and W. Nörenberg, *Eur. Phys. J. A* **15**, 375 (2002).
- [32] A. S. Umar, V. E. Oberacker, J. A. Maruhn, and P.-G. Reinhard, arXiv:nucl-th/0909.3469v1.
- [33] E. V. Prokhorova, E.A.Cherepanov, M.G.Itkis, et al, arXiv:nucl-ex/0309021.
- [34] A. J. Pacheco, J.O Fernandez Niello, D.E DiGregorio et al., *Phys. Rev. C* **45**, 2861 (1992).
- [35] Ning Wang, Xizhen Wu, et al., *Phys. Rev. C* **74**, 044604 (2006).